

1 **Novel Keeling plot based methods to estimate the isotopic composition of ambient water**
2 **vapor**

3 Yusen Yuan^{a,b}, Taisheng Du^{a*}, Honglang Wang^c, Lixin Wang^{b*}

4
5 ^a Center for Agricultural Water Research in China, China Agricultural University,
6 Beijing 100083, China

7 ^b Department of Earth Sciences, Indiana University-Purdue University Indianapolis,
8 Indianapolis, Indiana 46202, USA

9 ^c Department of Mathematical Sciences, Indiana University-Purdue University
10 Indianapolis, Indianapolis, Indiana 46202, USA

11
12 * Corresponding author: Dr. Taisheng Du
13 Fax: +86-10-62737611; Tel: +86-10-62738398
14 Email: dutaisheng@cau.edu.cn

15
16 * Corresponding author: Dr. Lixin Wang
17 Fax: +1-1-317-274-7966; Tel: +1-317-274-7764
18 Email: lxwang@iupui.edu

19
20
21 **Highlights:**

- 22 1. Two new methods were developed to estimate the isotopic composition of ambient
23 vapor.
- 24 2. Theoretical derivations were provided for these two methods.
- 25 3. Linear regression showed strong agreement between the two methods.
- 26 4. The methods provide a possibility to calculate the proportion of evapotranspiration
27 fluxes to total atmospheric vapor using the same instrumental setup for the traditional
28 Keeling plot investigations.

29

30 **Abstract**

31 Keeling plot approach, a general method to identify the isotopic composition of source
32 atmospheric CO₂ and water vapor (i.e., evapotranspiration), has been widely used in terrestrial
33 ecosystems. The isotopic composition of ambient water vapor (δ_a), an important source of
34 atmospheric water vapor, is not able to be estimated to date using the Keeling plot approach.
35 Here we proposed two new methods to estimate δ_a using the Keeling plots: one using
36 intersection point method and another relying on the Intermediate Value Theorem. As actual δ_a
37 value was difficult to measure directly, we used two indirect approaches to validate our new
38 methods. First, we made external vapor trackings using Hybrid Single Particle Lagrangian
39 Integrated Trajectory (HYSPLIT) model to facilitate explaining the variations of δ_a . The
40 trajectory vapor origin results were consistent with the expectations of the δ_a values estimated
41 by these two methods. Second, regression analysis was used to evaluate the relationship
42 between δ_a values estimated from these two independent methods and they are in strong
43 agreement. This study provides an analytical framework to estimate δ_a using existing facilities,
44 and provides important insights into the traditional Keeling plot approach by showing: a) a
45 possibility to calculate the proportion of evapotranspiration fluxes to total atmospheric vapor
46 using the same instrumental setup for the traditional Keeling plot investigations, and b)
47 perspectives on estimation of isotope composition of ambient CO₂ (δ_a^{13C}).

48

49 **Key words:** HYSPLIT, intersection point, Intermediate Value Theorem, Keeling plot, stable
50 isotope

51 **1. Introduction**

52 Stable isotopes of hydrogen and oxygen ($^1\text{H}^2\text{HO}$ and H_2^{18}O) have been widely used in
53 root water uptake source identification (Corneo et al., 2018, Mahindawansa et al., 2018,
54 Lanning et al., 2020) and evapotranspiration (ET) partitioning (Brunel et al., 1997; Wang et al.,
55 2010; Cui et al., 2020) in terrestrial ecosystems based on Craig-Gordon model (Craig and
56 Gordon, 1965), isotope mass balance and mechanisms of isotopic fractionation (Majoube, 1971;
57 Merlivat and Jouzel, 1979). With the advent of laser isotope spectrometry capable of high
58 frequency (1 Hz) measurements of the isotopic composition of atmospheric water vapor (δ_v)
59 and atmospheric water vapor content (C_v) (Kerstel and Gianfrani, 2008; Wang et al., 2009), the
60 number of studies based on high frequency ground-level isotope measurements was
61 continuously increasing. These studies generate new insights into the processes that affect δ_v ,
62 including meteorological factors (Galewsky et al., 2011; Steen-Larsen et al., 2013), biotic
63 factors (Wang et al., 2010) and multiple factors (Parkes et al., 2016). Such increase in δ_v
64 measurements allows an isotope-enabled global circulation models (Iso-GCMs) to estimate the
65 variation of water vapor isotope parameters at a global scale (Werner et al., 2011).
66 Concomitantly, more than δ_v , several new methods using high frequency ground-level isotope
67 measurements were devised to directly estimate the isotopic composition of leaf water (Song
68 et al., 2015) and leaf transpired vapor (Wang et al., 2012).

69 Evapotranspiration is a crucial component of water budget across scales such as field
70 (Wagle et al., 2020), watershed (Zhang et al., 2001), regional (Hobbins et al., 2001) and global
71 (Jung et al., 2010, Wang et al., 2014) scales. The water isotopic composition of ET (δ_{ET}) was
72 generally estimated by Keeling plot approach (Keeling, 1958). It was first used to explain

73 carbon isotope ratios of atmosphere CO₂ and to identify the sources that contribute to increases
74 in atmospheric CO₂ concentration, and has been further used to estimate δ_{ET} in recent two
75 decades (Yakir and Sternberg, 2000). Keeling plot analyses can be applied using δ_v and C_v
76 output by laser based analyzer either from different heights (Yepez et al., 2003; Zhang et al.,
77 2011; Good et al., 2012) or at one height with continuous observations (Wei et al., 2015;
78 Keppler et al., 2016). Although the intercept of the linear regression line was commonly used
79 as estimated δ_{ET} , the slope of the Keeling plot was also used to estimate δ_{ET} by re-arranging the
80 Keeling plot equations (Miller and Tans, 2003; Fiorella et al., 2018). Keeling plot approach was
81 based on isotope mass balance and two-source assumption using two equations with three
82 unknowns. As a result, the isotopic composition of other potential sources (e.g., water vapor
83 not from ET), as well as isotopic composition of ambient water vapor (δ_a), were not able to be
84 estimated directly using the Keeling plot approach. That is one of the reasons why field scale
85 moisture recycling is difficult to estimate to date.

86 In this study, we proposed two new methods to estimate δ_a , one based on the intersection
87 of two Keeling plots of two continuous observation moments and the other based on the
88 Intermediate Value Theorem. Proposition and proof were provided, and the new methods were
89 tested using field observations. As direct observations of δ_a rarely exist (Griffis et al., 2016),
90 we tested our methods by (a) making an external water vapor tracking investigation according
91 to HYSPLIT model to explain the variations of estimated δ_a , and (b) making a regression
92 analysis on daily scale and point to point scale using δ_a estimated by these two independent
93 methods.

116 this time interval, we have

$$117 \quad k_1 = C_a(\delta_a - \delta_{ET_1}) \quad , \quad (4)$$

$$118 \quad k_2 = C_a(\delta_a - \delta_{ET_2}) \quad , \quad (5)$$

119 where k_i and δ_{ET_i} represent the value at t_i for $i=1, 2$. From (4) and (5), we can solve δ_a as:

$$120 \quad \delta_a = \frac{k_1\delta_{ET_2} - k_2\delta_{ET_1}}{k_1 - k_2} \quad . \quad (6)$$

121 Algebraically, δ_a and C_a are solutions in Eq. (4) and Eq. (5). Geometrically, point $(\delta_a, 1/C_a)$ is

122 the intersection of two Keeling plots at t_1 and t_2 . That is the reason the method was named IP

123 method. The local constant approximation idea was first described in [Yamanaka and Shimizu](#)

124 [\(2007\)](#) as an assumption to quantify the contribution of local ET to total atmospheric vapor.

125 **Intermediate Value Theorem (IVT) method.** Denote the slope as $k = C_a(\delta_a - \delta_{ET})$.

126 Since $C_a < C_v = C_a + C_{ET}$, we have $C_a = \frac{k}{(\delta_a - \delta_{ET})} < C_v$. We can rearrange $\frac{k}{(\delta_a - \delta_{ET})} < C_v$

127 to attain δ_a : $\delta_a < \frac{k}{C_v} + \delta_{ET} = \delta_v$ when $k < 0$, and $\delta_a > \frac{k}{C_v} + \delta_{ET} = \delta_v$ when $k > 0$.

128 For the smooth function $\delta_a(t)$ defined on the interval $[t_1, t_2]$ with the two time points

129 satisfying $k(t_1)k(t_2) < 0$, depending on the sign of the slopes $k(t_1)$ and $k(t_2)$ and the order

130 of $\delta_{v_1} = \delta_v(t_1)$ and $\delta_{v_2} = \delta_v(t_2)$ at the two time points t_1 and t_2 , it will correspond to one

131 of the situations in **Fig. 1**. For all of the situations, by the Intermediate Value Theorem, there

132 exists a sub-interval $[t_1', t_2'] \subset [t_1, t_2]$ such that the whole range of $\{\delta_a(t): t \in [t_1', t_2']\}$ is

133 within $[\min(\delta_{v_1}, \delta_{v_2}), \max(\delta_{v_1}, \delta_{v_2})]$. Proof details of this proposition is shown in the

134 appendix. Thus for the two nearby time points t_1 and t_2 with k_1 and k_2 having different signs, δ_a

135 will be between δ_{v_1} and δ_{v_2} . This provides a prerequisite for estimating the parameter of

136 interest δ_a based on Intermediate Value Theorem, which leads to approximation of δ_a within the

137 time interval between t_1 and t_2 using δ_{v_1} and δ_{v_2} :

138
$$\delta_a \approx \frac{\delta_{v_1} + \delta_{v_2}}{2} \quad (7)$$

139 Using this method, we are able to compute δ_a using data points when the slopes of
140 Keeling plots change signs between two adjacent time points.

141 2.2 Field observations

142 2.2.1 Study site

143 A field measurement was conducted over a maize field (39 ha) from 1st May 2017 to 30st
144 September 2017 at Shiyanghe Experimental Station of China Agricultural University, located
145 in Wuwei of Gansu Province, northwest China (37°85'N, 102°88'E; altitude 1581m). The
146 region belongs to temperate continental climate and is in the oasis within the Shiyang river
147 basin. The annual mean temperature of the study area is about 8.8°C with pan evaporation of
148 2000 mm, annual precipitation of 164.4 mm, mean sunshine duration of 3000 h, and frost-free
149 period of more than 150 d. The local crops are irrigated using groundwater with electrical
150 conductivity of 0.62 dSm⁻¹. The groundwater table is 30-40 m below the surface. Maize was
151 sowed on April and harvested on September 2017, with row spacing of 40 cm and plant spacing
152 of 23 cm. The maize growing stage was divided into seedling stage (April 21st –May 20th),
153 jointing stage (May 21st-July 10th), heading period (July 11th-July 31st), pustulation period
154 (August 1st-August 31st) and mature period (September 1st-September 20th).

155 2.2.2 Instrument setup and measurement design

156 A 24-meter flux tower, located in the middle of maize field, was used to measure ET flux
157 and isotopic composition of water vapor at different heights. The field is approximately 600 m
158 long and 240 m wide, with a 10% slope decreasing from southwest to northeast. Five gas traps
159 were installed on the flux tower at heights of 4 m, 8 m, 12 m, 16 m and 20 m, respectively. An

160 iron pillar was placed 20 m away from the flux tower. Three gas traps were installed on the iron
161 pillar, one was close to the canopy, and the other two were 2 m and 3 m above the ground.
162 Canopy gas trap was adjusted weekly according to the height of maize.

163 *In situ* δ_v and C_v collected by the eight gas traps were monitored by a water vapor isotope
164 analyzer (L2130-i, Picarro Inc., Sunnyvale, CA, USA), which was a wavelength scanned cavity
165 ring down spectroscopy (WS-CRDS) instrument. Vapor specifications include a measurement
166 range from 1000 to 50000 ppm, the precision is 0.04‰ to 0.25‰ for $\delta^{18}\text{O}$ (Zhao et al., 2019).
167 Interfacing with the gas trap and the isotope analyzer, teflon tube was wrapped by thermal
168 insulation cotton to avoid vapor condensation during transmission. The measurement of δ_v and
169 C_v were conducted from May to September, which should have 153 days of data. Forty-nine
170 days among them were complete with 24-hour continuous datasets. There were missing data
171 for either a whole day or several hours of a day for other days due to the calibration and
172 maintenance of the analyzer. These 49 days were chosen in our study for data analysis.

173 2.2.3 Calibration of δ_v and C_v

174 Our calibration procedure mainly followed the study by Steen-Larsen et al. (2013) with
175 some modifications to fit our specific experimental setup. The water vapor from eight inlets
176 were sampled continuously over a 24-hour-period. Since only one analyzer was used to measure
177 the δ_v and C_v , the values of eight sampling inlets were recorded in turn every 225s in a 30 mins
178 cycle. The switch procedure was automatic. As the analyzer makes a measurement every 0.9-
179 1s, approximately 259-264 values for each inlet was recorded within the cycle. For each 225s
180 measurement period, No. 195 to No. 253 data points were used to avoid memory issue and
181 influence of transient pressure variation. The absolute value of coefficient of variations ($|CV|$)

182 of δ_v and C_v were no more than 0.016 and 0.002, respectively, which was far below the critical
183 value of 15% (Lovie, 2005). The mean value of the selected data points was regarded as the
184 measured δ_v and C_v in a specific inlet. Measured C_v was used directly as actual C_v , while
185 measured δ_v was calibrated to minimize the influence of isotopic concentration dependence.
186 The C_v in our measurement ranged from 5386 ppm to 30255 ppm. Thus, C_v gradients of 10000
187 ppm, 20000 ppm and 30000 ppm were selected as calibration concentrations to improve the
188 precision of δ_v . As we need continuous data, the observation should last uninterrupted as long
189 as possible. As a result, the calibration was made in every 5-10 days, which is consistent with
190 the frequency of calibration by other researchers such as Steen-Larsen et al. (2013). According
191 to our calibration data on standards, the average drift (absolute value) was about 0.16‰
192 between two adjacent calibrations.

193 2.3 Data quality control for δ_a estimation

194 With a 30-min interval for 49 days, we should in theory produce 2352 δ_a values for both
195 IP method and IVT method. However, because of the precondition of $k_1k_2 < 0$ required for the
196 IVT method, 166 δ_a values was able to be calculated using the IVT method ($\delta_{a(IVT)}$). δ_a values
197 using the IP method ($\delta_{a(IP)}$) was not restricted by this precondition. Furthermore, a filter
198 ($\delta_{ET} < \delta_v < \delta_a$ or $\delta_{ET} > \delta_v > \delta_a$) was used for both methods because δ_v was a mixture of δ_{ET} and δ_a .
199 Therefore, δ_a values that meet both precondition $k_1k_2 < 0$ and the condition of $\delta_{ET} < \delta_v < \delta_a$ or
200 $\delta_{ET} > \delta_v > \delta_a$ were considered satisfying the criteria for the IVT method; δ_a values that meet the
201 condition of $\delta_{ET} < \delta_v < \delta_a$ or $\delta_{ET} > \delta_v > \delta_a$ were considered satisfying the criteria for the IP method.
202 In the end, we obtained 1264 and 103 δ_a values using IP and IVT methods, respectively (Table
203 1). Eighty eight time points were overlapped between the IP and IVT based δ_a results. These 88

204 time points were selected to test the reliability of two methods at point to point scale. During
205 the 49 days, there were 21 days when more than one $\delta_{a(IVT)}$ was attained for each day. These 21
206 days was also used to investigate the time series of daily scale δ_a variations and other isotopic
207 variations. Further analysis in section 2.4 in the following was made on these 21 days.

208 2.4 Explanations of δ_a using backward trajectories

209 To explain the variations of estimated δ_a , air mass backward trajectories were calculated
210 using the Hybrid Single Particle Lagrangian Integrated Trajectory (HYSPLIT) model (Draxler
211 and Hess, 1997; Draxler, 2003; Stein et al., 2015; Kaseke et al., 2018) and meteorological data
212 from the Global Data Assimilation System 0.5 Degree (GDAS0p5) with $0.5^\circ \times 0.5^\circ$ spatial
213 resolution and 3-hour time resolution for the 21 days mentioned in section 2.3. Five hundred
214 meters height was selected in the modeling. Each backward trajectory was initialized from the
215 station ($37^\circ 85'N$, $102^\circ 88'E$) at 12:00 pm (local time), and calculated backward for 72 hours.
216 Eighteen trajectories were computed, except for June 21st, August 18th and September 29th when
217 vertical velocity data were missing. Finally, we used these 18 trajectories representing the vapor
218 origin in the corresponding 18 days.

219 3. Results

220 3.1 Time series variations of δ_{ET} , δ_v , δ_a and k

221 Time series of isotopic variations were shown in **Fig. 2**. The δ_v here is the average value
222 of eight heights. The average δ_{ET} , δ_v , $\delta_{a(IP)}$ and $\delta_{a(IVT)}$ were -11.04‰, -13.00‰, -13.60‰ and -
223 13.29‰, respectively in those 21 days when more than one $\delta_{a(IVT)}$ was attained for each day.
224 Daytime (7:00am-7:00pm) average δ_{ET} , δ_v , $\delta_{a(IP)}$ and $\delta_{a(IVT)}$ were -10.73‰, -13.33‰, -14.08‰
225 and -13.63‰, respectively. While at nighttime (7:00pm-7:00am the next day), average δ_{ET} was

226 lower than that at daytime, which was on the contrary with δ_v , $\delta_{a(IP)}$ and $\delta_{a(IVT)}$. The trend of $\delta_{a(IP)}$
227 and $\delta_{a(IVT)}$ were similar to δ_v . In majority of circumstances, δ_{ET} is the largest of those four
228 isotopic parameters, except on May 19th, June 4th and June 9th. About 76% of k values were
229 negative, and most positive k values occurred at nighttime (60%). The percentage of positive k
230 values were 33%, 34%, 24%, 34% and 10% in May, June, July, August and September,
231 respectively. Standard deviation was used here to evaluate the constancy among isotopic
232 parameters at daily scale. The standard deviation of δ_{ET} , δ_v , $\delta_{a(IP)}$ and $\delta_{a(IVT)}$ were 6.08‰, 0.91‰,
233 1.38‰ and 0.59‰, respectively. Therefore, the constancy of δ_a was similar to the constancy of
234 δ_v at daily scale.

235 3.2 Daily variations of HYSPLIT backward trajectories and δ_a using two methods

236 The 500 m height water vapor backward trajectories revealed that water vapor was from
237 outside the study regions for ten days (**Fig. 3a**), and water vapor was from local ET for eight
238 days (**Fig. 3b**).

239 As for the IP method, 53.7% of $\delta_{a(IP)}$ values met the criteria, and 49.4% of $\delta_{a(IP)}$ values
240 meeting the criteria were during the daytime (7:00am-7:00pm). The range of $\delta_{a(IP)}$ values
241 meeting the criteria were between -16.79‰ and -12.95‰ for the ten days with external origins
242 (**Fig. 3a**). The range of $\delta_{a(IP)}$ values meeting the criteria were between -12.77‰ and -9.51‰
243 for the eight days with local origins (**Fig. 3b**).

244 As for the IVT method, only 4.4% of δ_a values met the criteria, and 35.9% of δ_a values
245 meeting the criteria were during the daytime (7:00am-7:00pm). The range of $\delta_{a(IVT)}$ values
246 meeting the criteria were between -16.31‰ and -13.93‰ for the ten days with external origins
247 (**Fig. 3a**). The range of $\delta_{a(IVT)}$ values meeting the criteria were between -12.67‰ and -9.12‰

248 for the eight days with local origins (**Fig. 3b**).

249 3.3 Linear regression between $\delta_{a(IP)}$ and $\delta_{a(IVT)}$

250 Method comparison was made at both daily scale (**Fig. 4a**) and point to point scale (**Fig.**
251 **4b**). The 21 days (see method section 2.3) in **Fig. 3a** and **Fig. 3b** were selected to figure out the
252 daily scale relationship between $\delta_{a(IP)}$ and $\delta_{a(IVT)}$. Point to point scale data was based on the 88
253 point of overlapped $\delta_{a(IP)}$ and $\delta_{a(IVT)}$ (see method section 2.3) among all 49 days, which
254 accounted for 7.0% of δ_a values using IP method and 85.4% of δ_a values using IVT method.
255 Linear regression between $\delta_{a(IP)}$ and $\delta_{a(IVT)}$ was significant at both daily scale and point to point
256 scale. The degree of agreement was less for the daily time scale than point to point scale and
257 the RMES between these two methods at daily scale and point to point scale were 0.618‰ and
258 0.167‰, respectively.

259 4. Discussion

260 4.1 The reliability of δ_a estimating methods

261 The IP method was based on the assumption that the ambient sources were the same
262 between two continuous observation moments. This is a reasonable assumption for short time
263 intervals. For the IVT method, δ_a was derived from δ_v in two continuous moments when their
264 Keeling plot slopes were opposite. The opposite slopes of the Keeling plots were the only
265 requirement. As δ_v was almost constant in two continuously moments, $\delta_{a(IVT)}$ was able to be
266 constrained into a small range. The derivation was supported by the
267 Intermediate Value Theorem. Therefore, both methods of estimating δ_a were theoretically
268 sound.

269 The δ_a results were also examined by HYSPLIT backward trajectories to identify the

270 different sources of water vapor, which assesses the reliability of both methods indirectly. Based
 271 on the trajectory analysis, water vapor in the study area came from westerlies, northern polar
 272 region and local recirculation. Water vapor from southwest monsoon and northwest Pacific
 273 were not detected in this study. Based on the isotope variation of meteoric water (Fricke et al.,
 274 1999), water vapor from westerlies and northern polar was more ¹⁸O depleted than local
 275 recycled moisture through ET. It was also reported that the water vapor from outside the study
 276 regions will lower δ_v values (Ma et al., 2014; Chen et al., 2015). The calculated δ_a values of the
 277 ten days with external sources (Fig. 3a) based on the IP method and IVT approach were lower
 278 than those of eight days with local origin (Fig 3b), which was consistent with our expectation.
 279 The results indicate that quantifying δ_a using both the IP method and IVT approach was reliable.
 280 The reliability of two methods at point to point scale were also supported by the close
 281 relationship of δ_a using these two independent methods. Daily time scale result is less reliable
 282 than point to point scale.

283 4.2 The application of δ_a for moisture recycling

284 When δ_a was estimated, moisture recycling (e.g., f_{ET} , the contribution of ET fluxes to the
 285 total water vapor) can be estimated using the following equations with known δ_a , δ_{ET} , δ_v , C_{ET}
 286 and C_v :

$$287 \quad C_{ET} = C_v \cdot \frac{\delta_a - \delta_v}{\delta_a - \delta_{ET}} \quad , \quad (8)$$

$$288 \quad f_{ET} = \frac{C_{ET}}{C_v} \quad , \quad (9)$$

289 According to Eq. (8) and Eq. (9), f_{ET} was only related to δ_a , δ_v , and δ_{ET} . These three
 290 parameters were obtained for relatively small temporal and spatial scales in this study, making
 291 it possible to estimate f_{ET} at a tower scale. The f_{ET} estimate will provide a baseline value for

292 rainfall recycling ratio calculations. Previous studies quantified the contribution of recycled
293 vapor to annual or monthly precipitation in river basins using two-element mixture model (Kong
294 et al., 2013) and three-element mixture (Peng et al., 2011). At the watershed scale, recycled
295 vapor rate refers to the contributions of moisture from terrestrial ET to annual or monthly
296 precipitation (Trenberth, 1999). It is a key part of local water cycle and the atmospheric water
297 vapor balance (Seneviratne et al., 2006; Aemisegger et al., 2014). In our study, the role of f_{ET}
298 to regional vapor is similar to the role of recycled vapor rate to annual or monthly precipitation,
299 but f_{ET} was calculated with fine temporal (e.g., hourly) and spatial (i.e., field scale) scales. At
300 the watershed scale, assumption was made that no isotopic fractionation between transpiration
301 and source water (Flanagan et al., 1991); advected vapor was assumed to be the precipitation
302 vapor of the upwind station (Peng et al., 2011). However, the isotope composition of plant
303 transpired vapor is variable in a day especially under non-steady-state conditions (Farquhar and
304 Cernusak, 2005; Lai et al., 2008; Song et al., 2011). In addition, sometimes it is difficult to
305 select an upwind station without precipitation events. In this study, a field site was selected to
306 calculate the proportion of ET fluxes to total atmospheric vapor and f_{ET} was only related to δ_a ,
307 δ_v , and δ_{ET} according to Eq. (8) and Eq. (9). This indicates that f_{ET} calculations is possible for
308 fine temporal and spatial scales after estimating δ_a using the methods we proposed.

309 If we assumed that the parameter δ_v in Eq. (8) is the average δ_v value measured from all
310 the eight heights. f_{ET} in this study was 23.3% and 12.7% from May to September 2017 based
311 on daily $\delta_{a(IP)}$ and daily $\delta_{a(IVT)}$, respectively. It was reported that recycled vapor rate in all
312 Shiyang river basin, oasis region, mountain region and desert region were 23%, 28%, 17% and
313 15%, respectively (Li, et al., 2016; Zhu, et al., 2019). The f_{ET} based on daily $\delta_{a(IP)}$ in our study

314 was close to these earlier studies. The deviation of f_{ET} based on daily $\delta_{a(IVT)}$ from previous
315 studies may be because 64.1% of point to point $\delta_{a(IVT)}$ was observed at nighttime. Normally, ET
316 at nighttime is lower than that of daytime. f_{ET} may be underestimated using daily $\delta_{a(IVT)}$. It could
317 also be inferred that f_{ET} estimation using Eq. (9) may be more reliable using daily $\delta_{a(IP)}$ than
318 daily $\delta_{a(IVT)}$.

319 4.3 Implications of δ_a

320 The signature of δ_E and δ_T was first introduced by a hypothetical graph shown on **Fig.**
321 **5a** (Moreira et al., 1997). Line 1 and line 2 was idealized Keeling plot with pure T and pure E,
322 and Line 3 was the Keeling plot with mixed T and E. The IVT method in this study provided a
323 general explanation of this figure. As T is a major component of ET in the daytime in non-arid
324 region (Wang et al., 2014), the slope is generally negative. When E dominates ET in an
325 ecosystem, such as in the nighttime in non-arid region or in arid region, the slope should be
326 positive. Mathematically, negative slope is due to $\delta_{ET} > \delta_a$ and positive slope is due to $\delta_{ET} < \delta_a$.
327 It also reflected that IVT method could only be used in non-arid ecosystems to ensure the
328 occurrence of sign switch (e.g., from negative to positive) in Keeling plot slopes. On the
329 contrary, IP method may not be restricted by the type of ecosystems. Yamanaka and Shimizu
330 (2007) used the assumption that δ_a of an area of 219.9 km² was represented by the intersection
331 point of two Keeling plot lines in different sites with synchronous measurements and they used
332 the intersection value as an approximate value of δ_a . This study was conducted in a maize field
333 using 30-min interval measurements. The results verified Yamanaka and Shimizu's (2007)
334 assumption in such fine spatial and temporal scale, and indicate that accurate $\delta_{a(IP)}$ could be
335 estimated from the intersection of two Keeling plots regardless the slope being positive or

336 negative, while the $\delta_{a(IVT)}$ should be restricted in the area between two dotted lines as shown in
337 **Fig. 5b** (i.e., between the minimum value of δ_v in positive slope and the maximum value of δ_v
338 in negative slope). Although IVT method relies on more stringent precondition for data filtering,
339 this method requires a very simple expression, which only needs two parameters to be measured
340 according to Eq. (7).

341 While this study is about water vapor ^{18}O , the “Keeling plot” was first used by Keeling
342 (1958, 1961) to interpret carbon isotope ratios of mixed CO_2 and to identify the sources that
343 contribute to increases in atmospheric CO_2 concentrations on a regional basis. Compared with
344 ET in water vapor which consists of E and T, net ecosystem CO_2 exchange is comprised of soil
345 respiration (R) and gross primary productivity (GPP). As $^{13}\text{CO}_2$ isotopic Keeling plot reveals a
346 positive slope during both daytime and nighttime (Yakir and Wang, 1996; Unger et al., 2010),
347 the IVT method may not be able to estimate ambient $^{13}\text{CO}_2$ isotopic composition ($\delta_a^{13}\text{C}$) since
348 there are no opposite slopes in a day. In such case, the IP method may be implemented in two
349 continuous moments to estimate $\delta_a^{13}\text{C}$ and may consequently further calculate the contribution
350 of Net Ecosystem Exchange (NEE) to atmospheric CO_2 .

351 5. Conclusions

352 In this study, we established two methods to quantify δ_a using intersection point method
353 and the Intermediate Value Theorem method. The IVT method was used under the condition of
354 opposite slope of Keeling plots in two continuously moments. The results of estimated $\delta_{a(IP)}$ and
355 $\delta_{a(IVT)}$ were consistent with the expectation whether it was local origin or external origin using
356 external vapor tracking investigation by HYSPLIT model. The linear regression between $\delta_{a(IP)}$
357 and $\delta_{a(IVT)}$ was highly significant at both daily time scale and point to point scale.

358 This study provided insights into the underexplored traditional Keeling plots and
359 provided two methods to estimate δ_a using the same instrumental setup for the traditional
360 Keeling plot investigations. The estimated δ_a will make it possible to calculate the ET
361 contribution to regional vapor at a 30 min interval at field scale. The results also indicate that
362 using similar framework, δ_a^{13C} may also solvable by the IP method.

363 **6. Acknowledgements**

364 We acknowledge support from the National Natural Science Foundation of China
365 (51725904, 51621061, 51861125103), the National Key Research Program
366 (2016YFC0400207), the Discipline Innovative Engineering Plan (111 Program, B14002), the
367 Graduate International Training and Promotion Program of China Agricultural University
368 (31051521), and the President's International Research Awards from Indiana University and
369 the Division of Earth Sciences of National Science Foundation (EAR-1554894). We thank Dr.
370 Qianning Liu from Jiangxi University of Finance and Economics and Dr. Zhengxiang Chen
371 from Capital Normal University for checking the validity of the Intermediate Value Theorem
372 method.

373 **7. Code and Data availability**

374 Code and data are available on request.

375 **8. Author contribution**

376 YY, TD and LW conceptualized the main research questions. YY collected data
377 and performed the data analyses. YY and LW wrote the first draft. HW contributed to
378 additional data analyses. All the authors contributed ideas and edited the manuscript.

379 **9. Competing interests**

380 There authors declare no competing interests.

381 **10. References**

- 382 Aemisegger, F., Pfahl, S., Sodemann, H., Lehner, I., Seneviratne, S. I., and Wernli, H.:
383 Deuterium excess as a proxy for continental moisture recycling and plant transpiration,
384 **Atmospheric Chemistry and Physics**, 14, 4029–4054, doi: 10.5194/acp-144029-2014, 2014.
- 385 Brunel, J. P., Walker, G. R., Dighton, J. C., and Monteny, B.: Use of stable isotopes of water to
386 determine the origin of water used by the vegetation and to partition evapotranspiration. A
387 case study from HAPEX-Sahel, **Journal of Hydrology**, 188–189, 466–481,
388 doi:10.1016/s0022-1694(96)03188-5, 1997.
- 389 Chen, F. L., Zhang, M. J., Ma, Q., Wang, S. J., Li, X. F., and Zhu, X. F.: Stable isotopic
390 characteristics of precipitation in Lanzhou city and its surrounding areas, Northwest China,
391 **Environmental Earth Sciences**, 73, 4671–4680, doi: 10.1007/s12665-014-3776-6, 2015.
- 392 Corneo, P. E., Kertesz, M. A., Bakhshandeh, S., Tahaei, H., Barbour, M. M., and Dijkstra, F. A.:
393 Studying root water uptake of wheat genotypes in different soils using water $\delta^{18}\text{O}$ stable
394 isotopes, **Agriculture, Ecosystems & Environment**, 264, 119-129, doi:
395 10.1016/j.agee.2018.05.007, 2018.
- 396 Craig, H. and Gordon, L. I.: Deuterium and oxygen 18 variations in the ocean and marine
397 atmosphere, in: **Stable Isotopes in Oceanographic Studies and Paleotemperatures**, p. 9,
398 1965.
- 399 Cui, J., Tian, L., Wei, Z., Huntingford, C., Wang, P., Cai, Z., Ma, N., and Wang, L.: Quantifying
400 the controls on evapotranspiration partitioning in the highest alpine meadow ecosystems,
401 **Water Resources Research**, 56, doi: 10.1029/2019WR024815, 2020.
- 402 Draxler, R. R., and Hess, G.: Description of the HYSPLIT4 modeling system, **NOAA Tech**
403 **Memo ERL ARL-224**, Dec, 24p., 1997.
- 404 Draxler, R. R.: Evaluation of an ensemble dispersion calculation, **Journal of Applied**
405 **Meteorology**, 42, 308-317, doi: 10.1175/1520-0450(2003)042<0308:EOAEDC>2.0.CO;2,
406 2003.
- 407 Farquhar, G. D., and Cernusak, L. A.: On the isotopic composition of leaf water in the non-
408 steady state, **Functional Plant Biology**, 32(4), 293-303, doi: 10.1071/FP04232, 2005.
- 409 Fiorella, R. P., Poulsen, C. J., and Matheny, A. M.: Seasonal patterns of water cycling in a deep,
410 continental mountain valley inferred from stable water vapor isotopes, **Journal of**
411 **Geophysical Research: Atmospheres**, 123, 7271-7291, doi: 10.1029/2017JD028093, 2018.
- 412 Flanagan, L. B., Comstock, J. P., and Ehleringer, J. R.: Comparison of modeled and observed
413 environmental influences on the stable oxygen and hydrogen isotope composition of leaf
414 water in *Phaseolus vulgaris* L, **Plant Physiology**, 96, 588-596, doi:
415 https://doi.org/10.1104/pp.96.2.588, 1991.
- 416 Fricke, H. C., O'Neil, J. R. J. E., and Letters, P. S.: The correlation between $^{18}\text{O}/^{16}\text{O}$ ratios of
417 meteoric water and surface temperature: its use in investigating terrestrial climate change over
418 geologic time, **Earth and Planetary Science Letters**, 170, 181-196, doi: 10.1016/S0012-
419 821X(99)00105-3, 1999.

420 Galewsky, J., Rella, C., Sharp, Z., Samuels, K., and Ward, D.: Surface measurements of upper
421 tropospheric water vapor isotopic composition on the Chajnantor Plateau, Chile, **Geophysical**
422 **Research Letters**, 38, 1-5, doi: 10.1029/2011GL048557, 2011.

423 Good, S. P., Soderberg, K., Wang, L., and Caylor, K. K.: Uncertainties in the assessment of the
424 isotopic composition of surface fluxes: A direct comparison of techniques using laser-based
425 water vapor isotope analyzers, **Journal of Geophysical Research: Atmospheres**, 117, doi:
426 10.1029/2011JD017168, 2012.

427 Griffis, T. J., Wood, J. D., Baker, J. M., Lee, X., Xiao, K., Chen, Z., Welp, L. R., Schultz, N. M.,
428 Gorski, G., and Chen, M.: Investigating the source, transport, and isotope composition of
429 water vapor in the planetary boundary layer, **Atmospheric Chemistry and Physics**, 16,
430 5139-5157, doi: 10.5194/acp-16-5139-2016, 2016.

431 Hobbins, M. T., Ramirez, J. A., and Brown, T. C.: The complementary relationship in estimation
432 of regional evapotranspiration: An enhanced advection-aridity model, **Water Resources**
433 **Research**, 37, 1389-1403, doi: 10.1029/2000WR900359, 2001.

434 Jung, M., Reichstein, M., Ciais, P., Seneviratne, S. I., Sheffield, J., Goulden, M. L., Bonan, G.,
435 Cescatti, A., Chen, J., and De Jeu, R.: Recent decline in the global land evapotranspiration
436 trend due to limited moisture supply, **Nature**, 467, 951-954, doi: 10.1038/nature09396, 2010.

437 Kaseke, K. F., Wang, L., Wanke, H., Tian, C., Lanning, M., and Jiao, W.: Precipitation origins
438 and key drivers of precipitation isotope (^{18}O , ^2H , and ^{17}O) compositions over windhoek,
439 **Journal of Geophysical Research: Atmospheres**, 123, 7311-7330, doi:
440 10.1029/2018JD028470, 2018.

441 Keeling, C. D.: The concentration and isotopic abundances of atmospheric carbon dioxide in
442 rural areas, **Geochimica et Cosmochimica Acta**, 13, 322-334, doi: 10.1016/0016-
443 7037(58)90033-4, 1958.

444 Keeling, C. D.: The concentration and isotopic abundances of carbon dioxide in rural and marine
445 air, **Geochimica et Cosmochimica Acta**, 24, 277-298, doi: 10.1016/0016-7037(61)90023-0,
446 1961.

447 Keppler, F., Schiller, A., Ehehalt, R., Greule, M., Hartmann, J., and Polag, D.: Stable isotope and
448 high precision concentration measurements confirm that all humans produce and exhale
449 methane, **Journal of Breath Research**, 10, 016003, doi: 10.1088/1752-7155/10/1/016003,
450 2016.

451 Kerstel, E., and Gianfrani, L.: Advances in laser-based isotope ratio measurements: selected
452 applications, **Applied Physics B**, 92, 439-449, doi: 10.1007/s00340-008-3128-x, 2008.

453 Kong, Y., Pang, Z., and Froehlich, K.: Quantifying recycled moisture fraction in precipitation of
454 an arid region using deuterium excess, **Tellus B: Chemical and Physical Meteorology**, 65,
455 19251, doi: 10.3402/tellusb.v65i0.19251, 2013.

456 Lai, C.T., Ometto, J. P., Berry, J. A., Martinelli, L. A., Domingues, T. F., and Ehleringer, J. R.:
457 Life form-specific variations in leaf water oxygen-18 enrichment in Amazonian vegetation,
458 **Oecologia**, 157, 197-210, doi: 10.1007/s00442-008-1071-5, 2008.

459 Lanning, M., Wang, L., Benson, M., Zhang, Q., and Novick, K. A.: Canopy isotopic
460 investigation reveals different water uptake dynamics of maples and oaks, **Phytochemistry**,
461 175, 112389, doi:10.1016/j.phytochem.2020.112389, 2020.

462 Li, Z., Feng, Q., Wang, Q., Kong, Y., Chen, A., Song, Y., Li, Y., Li, J., and Guo, X.:
463 Contributions of local terrestrial evaporation and transpiration to precipitation using $\delta^{18}\text{O}$ and

464 D-excess as a proxy in Shiyang inland river basin in China, **Global and Planetary Change**,
465 146, 140-151, doi: 10.1016/j.gloplacha.2016.10.003, 2016.

466 Lovie, P.: Coefficient of variation, **Encyclopedia of Statistics in Behavioral Science**, doi:
467 10.1002/0470013192.bsa107, 2005.

468 Ma, Q., Zhang, M., Wang, S., Wang, Q., Liu, W., Li, F., and Chen, F.: An investigation of
469 moisture sources and secondary evaporation in Lanzhou, Northwest China, **Environmental**
470 **Earth Sciences**, 71, 3375-3385, doi: 10.1007/s12665-013-2728-x, 2014.

471 Mahindawansa, A., Orlowski, N., Kraft, P., Rothfuss, Y., Racela, H., and Breuer, L.:
472 Quantification of plant water uptake by water stable isotopes in rice paddy systems, **Plant**
473 **and Soil**, 429, 281-302, doi: 10.1007/s11104-018-3693-7, 2018.

474 Majoube, M.: Fractionnement en oxygene 18 et en deuterium entre l'eau et sa vapeur, **Journal**
475 **de Chimie Physique**, 68, 1423-1436, doi: 10.1051/jcp/1971681423, 1971.

476 Merlivat, L., and Jouzel, J.: Global climatic interpretation of the deuterium-oxygen 18
477 relationship for precipitation, **Journal of Geophysical Research: Oceans**, 84, 5029-5033,
478 doi: 10.1029/JC084iC08p05029, 1979.

479 Miller, J. B., and Tans, P. P.: Calculating isotopic fractionation from atmospheric measurements
480 at various scales, **Tellus B**, 55, 207-214, doi: 10.1034/j.1600-0889.2003.00020.x, 2003.

481 Moreira, M., Sternberg, L., Martinelli, L., Victoria, R., Barbosa, E., Bonates, L., and Nepstad,
482 D.: Contribution of transpiration to forest ambient vapour based on isotopic measurements,
483 **Global Change Biology**, 3, 439-450, doi: 10.1046/j.1365-2486.1997.00082.x, 1997.

484 Parkes, S., McCabe, M., Griffiths, A. D., Wang, L., Chambers, S., Ershadi, A., Williams, A. G.,
485 Strauss, J., and Element, A.: Response of water vapour D-excess to land-atmosphere
486 interactions in a semi-arid environment, **Hydrology and Earth System Sciences**, 21, 533-548,
487 doi:10.5194/hess-21-533-2017, 2016.

488 Peng, T. R., Liu, K. K., Wang, C. H., and Chuang, K. H.: A water isotope approach to assessing
489 moisture recycling in the island-based precipitation of Taiwan: A case study in the western
490 Pacific, **Water Resources Research**, 47, W08507, doi: 10.1029/2010WR009890, 2011.

491 Seneviratne, S. I., Lüthi, D., Litschi, M., and Schär, C.: Land-atmosphere coupling and climate
492 change in Europe, **Nature**, 443, 205-209, doi: 10.1038/nature05095, 2006.

493 Song, X., Barbour, M. M., Saurer, M., and Helliker, B. R.: Examining the large-scale
494 convergence of photosynthesis-weighted tree leaf temperatures through stable oxygen isotope
495 analysis of multiple data sets, **New Phytologist**, 192: 912-924, doi: 10.1111/j.1469-
496 8137.2011.03851.x, 2011.

497 Song, X., Simonin, K. A., Loucos, K. E., and Barbour, M. M.: Modelling non-steady-state
498 isotope enrichment of leaf water in a gas-exchange cuvette environment, **Plant, Cell &**
499 **Environment**, 38, 2618-2628, doi: 10.1111/pce.12571, 2015.

500 Steen-Larsen, H. C., Johnsen, S. J., Masson-Delmotte, V., Stenni, B., Risi, C., Sodemann, H.,
501 Balslev-Clausen, D., Blunier, T., Dahl-Jensen, D., and Ellehøj, M. D.: Continuous monitoring
502 of summer surface water vapor isotopic composition above the Greenland Ice Sheet,
503 **Atmospheric Chemistry and Physics**, 13, 4815-4828, doi:10.5194/acp-13-4815-2013, 2013.

504 Stein, A., Draxler, R. R., Rolph, G. D., Stunder, B. J., Cohen, M., and Ngan, F.: NOAA's
505 HYSPLIT atmospheric transport and dispersion modeling system, **Bulletin of the American**
506 **Meteorological Society**, 96, 2059-2077, doi: 10.1175/BAMS-D-14-00110.1, 2015.

507 Trenberth, K. E.: Atmospheric moisture recycling: Role of advection and local evaporation,

508 **Journal of Climate**, 12, 1368-1381, doi: 10.1175/15200442(1999)012<1368:AMRROA>2.0.
509 CO₂;2, 1999.

510 Unger, S., Máguas, C., Pereira, J. S., Aires, L. M., David, T. S., and Werner, C.: Disentangling
511 drought-induced variation in ecosystem and soil respiration using stable carbon isotopes,
512 **Oecologia**, 163, 1043-1057, doi: 10.1007/s00442-010-1576-6, 2010.

513 Wagle, P., Skaggs, T. H., Gowda, P. H., Northup, B. K., and Neel, J. P.: Flux variance similarity-
514 based partitioning of evapotranspiration over a rainfed alfalfa field using high frequency eddy
515 covariance data, **Agricultural and Forest Meteorology**, 285, 107907, doi:
516 10.1016/j.agrformet.2020.107907, 2020.

517 Wang, L., Caylor, K. K., and Dragoni, D.: On the calibration of continuous, high-precision $\delta^{18}\text{O}$
518 and $\delta^2\text{H}$ measurements using an off-axis integrated cavity output spectrometer, **Rapid**
519 **Communications in Mass Spectrometry**, 23, 530-536, doi: 10.1002/rcm.3905, 2009.

520 Wang, L., Caylor, K. K., Villegas, J. C., Barron-Gafford, G. A., Breshears, D. D., and Huxman,
521 T. E.: Partitioning evapotranspiration across gradients of woody plant cover: Assessment of a
522 stable isotope technique, **Geophysical Research Letters**, 37, L09401, doi:
523 10.1029/2010GL043228, 2010.

524 Wang, L., Good, S. P., Caylor, K. K., and Cernusak, L. A.: Direct quantification of leaf
525 transpiration isotopic composition, **Agricultural and Forest Meteorology**, 154-155, 127-
526 135, doi: 10.1016/j.agrformet.2011.10.018, 2012.

527 Wang, L., Niu, S., Good, S. P., Soderberg, K., McCabe, M. F., Sherry, R. A., Luo, Y., Zhou, X.,
528 Xia, J., and Caylor, K. K.: The effect of warming on grassland evapotranspiration partitioning
529 using laser-based isotope monitoring techniques, **Geochimica et Cosmochimica Acta**, 111,
530 28-38, doi: 10.1016/j.gca.2012.12.047, 2013.

531 Wang, L., Good, S. P., and Caylor, K. K.: Global synthesis of vegetation control on
532 evapotranspiration partitioning, **Geophysical Research Letters**, 41, 6753–6757,
533 10.1002/2014GL061439, 2014.

534 Wei, Z., Yoshimura, K., Okazaki, A., Kim, W., Liu, Z., and Yokoi, M.: Partitioning of
535 evapotranspiration using high-frequency water vapor isotopic measurement over a rice paddy
536 field, **Water Resources Research**, 51, 3716-3729, doi: 10.1002/2014WR016737, 2015.

537 Werner, M., Langebroek, P. M., Carlsen, T., Herold, M., and Lohmann, G.: Stable water isotopes
538 in the ECHAM5 general circulation model: Toward high-resolution isotope modeling on a
539 global scale, **Journal of Geophysical Research: Atmospheres**, 116, D15109,
540 doi:10.1029/2011JD015681, 2011.

541 Yakir, D., and Wang, X.F.: Fluxes of CO₂ and water between terrestrial vegetation and the
542 atmosphere estimated from isotope measurements, **Nature**, 380, 515-517, doi:
543 10.1038/380515a0, 1996.

544 Yakir, D., and Sternberg, L.: The use of stable isotopes to study ecosystem gas exchange,
545 **Oecologia**, 123, 297-311, doi: 10.1007/s004420051016, 2000.

546 Yamanaka, T., and Shimizu, R.: Spatial distribution of deuterium in atmospheric water vapor:
547 Diagnosing sources and the mixing of atmospheric moisture, **Geochimica et Cosmochimica**
548 **Acta**, 71, 3162-3169, doi: 10.1016/j.gca.2007.04.014, 2007.

549 Yepez, E. A., Williams, D. G., Scott, R. L., and Lin, G.: Partitioning overstory and understory
550 evapotranspiration in a semiarid savanna woodland from the isotopic composition of water
551 vapor, **Agricultural and Forest Meteorology**, 119, 53-68, doi: 10.1016/S0168-

552 1923(03)00116-3, 2003.
553 Zhang, L., Dawes, W., and Walker, G.: Response of mean annual evapotranspiration to
554 vegetation changes at catchment scale, **Water Resources Research**, 37, 701-708, doi:
555 10.1029/2000WR900325, 2001.
556 Zhang, Y., Shen, Y., Sun, H., and Gates, J. B.: Evapotranspiration and its partitioning in an
557 irrigated winter wheat field: A combined isotopic and micrometeorologic approach, **Journal**
558 **of Hydrology**, 408, 203-211, doi: 10.1016/j.jhydrol.2011.07.036, 2011.
559 Zhao, L., Liu, X., Wang, N., Kong, Y., Song, Y., He, Z., Liu, Q., and Wang, L.: Contribution of
560 recycled moisture to local precipitation in the inland Heihe River Basin, **Agricultural and**
561 **Forest Meteorology**, 271, 316-335, doi: 10.1016/j.agrformet.2019.03.014, 2019.
562 Zhu, G., Guo, H., Qin, D., Pan, H., Zhang, Y., Jia, W., and Ma, X.: Contribution of recycled
563 moisture to precipitation in the monsoon marginal zone: Estimate based on stable isotope
564 data, **Journal of Hydrology**, 569, 423-435, doi: 10.1016/j.jhydrol.2018.12.014, 2019.
565

566 11. Appendix

567 **Proposition.** In the traditional linear Keeling plot system, denote $\delta_a = f(t)$, $\delta_v = g(t)$,
568 $\delta_{ET} = h(t)$ and $C_a = I(t) > 0$ as continuous functions of time. And for two definite
569 moments t_1 and t_2 ($t_1 < t_2$), $\delta_{a_1} \neq \delta_{a_2} \neq \delta_{v_1} \neq \delta_{v_2} \neq \delta_{ET_1} \neq \delta_{ET_2}$. The slopes of
570 corresponding keeling plot curve are $k_1 = C_{a_1}(\delta_{a_1} - \delta_{ET_1})$ and $k_2 = C_{a_2}(\delta_{a_2} - \delta_{ET_2})$,
571 respectively. Then we have that when $k_1 k_2 < 0$, there exists $[t_1', t_2'] \subset [t_1, t_2]$, such that
572 $[\min(f(t_1'), f(t_2')), \max(f(t_1'), f(t_2'))] \subset [\min(\delta_{v_1}, \delta_{v_2}), \max(\delta_{v_1}, \delta_{v_2})]$.

573 **Remark:** To make a proof of the proposition, classical Intermediate Value Theorem (IVT)
574 was used. It states that if f is a continuous function from the interval $I = [a, b]$ to real number
575 (R). Then *Version I.* if u is a number between $f(a)$ and $f(b)$, there is c in (a, b) such that $f(c) =$
576 u . *Version II.* the image set $f(I)$ is also an interval, and it contains
577 $[\min(f(a), f(b)), \max(f(a), f(b))]$. While in this study, IVT was able to be explained as
578 follows: if f is a continuous function from the interval $I = [t_1, t_2]$ to R with
579 $\min[f(t_1), f(t_2)] < \delta_v$ and $\max[f(t_1), f(t_2)] > \delta_v$, then *Version I* implies that there is t'
580 $\in (t_1, t_2)$ such that $f(t') = \delta_v$. And *Version II* implies that the image set $f(I)$ is also an

581 interval, and it contains $[\min(f(t_1), f(t_2)), \max(f(t_1), f(t_2))]$.

582 **Proof.** Since $k_1 k_2 < 0$, we have $\delta_{a_1} < \delta_{v_1}$ and $\delta_{a_2} > \delta_{v_2}$, or $\delta_{a_1} > \delta_{v_1}$ and $\delta_{a_2} <$
583 δ_{v_2} . As a result, the cases $\delta_{a_1} < \delta_{v_1} < \delta_{a_2} < \delta_{v_2}$, $\delta_{v_1} < \delta_{a_1} < \delta_{v_2} < \delta_{a_2}$, $\delta_{v_2} < \delta_{a_2} <$
584 $\delta_{v_1} < \delta_{a_1}$, $\delta_{a_2} < \delta_{v_2} < \delta_{a_1} < \delta_{v_1}$ and $[\min(\delta_{v_1}, \delta_{v_2}), \max(\delta_{v_1}, \delta_{v_2})] \cap$
585 $[\min(\delta_{a_1}, \delta_{a_2}), \max(\delta_{a_1}, \delta_{a_2})] = \emptyset$ do not meet the precondition $k_1 k_2 < 0$. There are only
586 four cases below. We will prove the proposition in each of the four cases.

587 Case 1: $[\min(\delta_{v_1}, \delta_{v_2}), \max(\delta_{v_1}, \delta_{v_2})] \subset [\min(\delta_{a_1}, \delta_{a_2}), \max(\delta_{a_1}, \delta_{a_2})]$ (**Fig. 1 a**).

588 According to IVT *Version I*, there exists $t_1' \in [t_1, t_2]$, such that $f(t_1') = \delta_{v_1}$;
589 similarly, there exists $t_2' \in [t_1, t_2]$, such that $f(t_2') = \delta_{v_2}$. Based on IVT *Version II*, there
590 exists $[t_1', t_2'] \subset [t_1, t_2]$, such that $[\min(f(t_1'), f(t_2')), \max(f(t_1'), f(t_2'))] =$
591 $[\min(\delta_{v_1}, \delta_{v_2}), \max(\delta_{v_1}, \delta_{v_2})]$.

592 Case 2: $[\min(\delta_{a_1}, \delta_{a_2}), \max(\delta_{a_1}, \delta_{a_2})] \subset [\min(\delta_{v_1}, \delta_{v_2}), \max(\delta_{v_1}, \delta_{v_2})]$ (**Fig. 1 b**).

593 According to IVT *Version I*, there exists $t_1' \in [t_1, t_2]$, such that $f(t_1') = \delta_{a_1}$;
594 similarly, there exists $t_2' \in [t_1, t_2]$, such that $f(t_2') = \delta_{a_2}$. Based on IVT *Version II*, there
595 exists $[t_1', t_2'] \subset [t_1, t_2]$, such that $[\min(f(t_1'), f(t_2')), \max(f(t_1'), f(t_2'))] =$
596 $[\min(\delta_{a_1}, \delta_{a_2}), \max(\delta_{a_1}, \delta_{a_2})] \subset [\min(\delta_{v_1}, \delta_{v_2}), \max(\delta_{v_1}, \delta_{v_2})]$.

597 Case 3: $\delta_{v_2} < \delta_{a_1} < \delta_{v_1} < \delta_{a_2}$, or $\delta_{a_2} < \delta_{v_1} < \delta_{a_1} < \delta_{v_2}$ (**Fig. 1 c and Fig. 1 d**).

598 According to IVT *Version I*, there exists $t_2' \in [t_1, t_2]$, such that $f(t_2') = \delta_{v_1}$.
599 Given case (2), when $[\min(\delta_{a_1}, \delta_{v_1}), \max(\delta_{a_1}, \delta_{v_1})] \subset [\min(\delta_{v_1}, \delta_{v_2}), \max(\delta_{v_1}, \delta_{v_2})]$, there
600 exists $[t_1', t_2'] \subset [t_1, t_2]$, such that $[\min(f(t_1'), f(t_2')), \max(f(t_1')$
601 $), f(t_2'))] \subset [\min(\delta_{a_1}, \delta_{v_1}), \max(\delta_{a_1}, \delta_{v_1})] \subset [\min(\delta_{v_1}, \delta_{v_2}), \max(\delta_{v_1}, \delta_{v_2})]$.

602 Case 4: $\delta_{v_1} < \delta_{a_2} < \delta_{v_2} < \delta_{a_1}$, or $\delta_{a_1} < \delta_{v_2} < \delta_{a_2} < \delta_{v_1}$ (**Fig. 1 e and Fig. 1 f**).

603 According to IVT Version I, there exists $t_1' \in [t_1, t_2]$, such that $f(t_1') = \delta_{v_2}$. Based
604 on case (2), when $[\min(\delta_{a_2}, \delta_{v_2}), \max(\delta_{a_2}, \delta_{v_2})] \subset [\min(\delta_{v_1}, \delta_{v_2}), \max(\delta_{v_1}, \delta_{v_2})]$, there
605 exists $[t_1', t_2'] \subset [t_1', t_2] \subset [t_1, t_2]$, such that $[\min(f(t_1'), f(t_2')), \max(f(t_1'$
606 $), f(t_2'))] \subset [\min(\delta_{a_2}, \delta_{v_2}), \max(\delta_{a_2}, \delta_{v_2})] \subset [\min(\delta_{v_1}, \delta_{v_2}), \max(\delta_{v_1}, \delta_{v_2})]$.

607 Thus the proposition is true for all four possible scenarios, which make the estimation of
608 δ_a theoretically feasible when $k_1 k_2 < 0$ and δ_{v_1} and δ_{v_2} adequately close. Actual δ_a
609 between t_1 and t_2 can be ensured in the interval $[\min(\delta_{v_1}, \delta_{v_2}), \max(\delta_{v_1}, \delta_{v_2})]$.
610 To simplify the result, actual δ_a between t_1 and t_2 can be approximately regarded as what Eq. (7)
611 reveals.

612

613

614

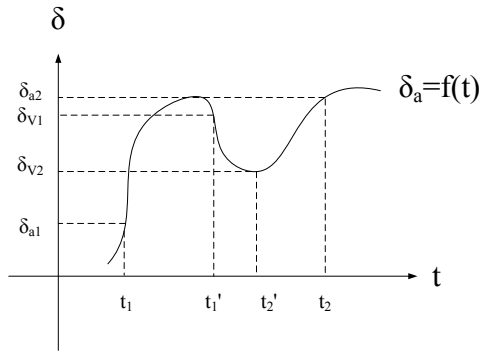
615

616

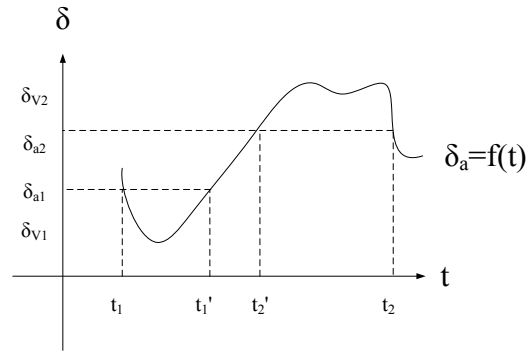
617 Table 1. The number of estimated isotope composition of ambient vapor meeting the criteria
 618 using the intersection point method ($\delta_{a(IP)}$) and the Intermediate Value Theorem method ($\delta_{a(IVT)}$)
 619 among all 49 days.

Date	number of $\delta_{a(IP)}$ values	number of $\delta_{a(IVT)}$ values
	meeting the criteria in a whole day	meeting the criteria in a whole day
5/19	27	8
5/27	13	3
5/28	30	3
5/31	25	5
6/4	38	5
6/5	28	0
6/7	29	6
6/9	32	5
6/10	26	2
6/11	21	4
6/12	22	4
6/15	32	0
6/16	33	0
6/17	24	1
6/18	26	0
6/21	26	3
6/22	22	0
6/26	22	0
6/27	29	3
7/4	23	0
7/5	23	1
7/7	30	0
7/8	29	0
7/14	28	4
7/16	28	0
7/18	25	1
7/19	28	6
7/20	27	6
7/21	29	0
7/22	19	0
8/3	18	1
8/4	22	3
8/5	25	3
8/6	28	1
8/12	13	8
8/18	19	3
8/19	30	0
8/28	23	0
8/29	22	1
8/30	27	1
8/31	27	0
9/20	25	0
9/21	24	1
9/22	31	1
9/23	28	1
9/27	28	2
9/28	25	1
9/29	30	5
9/30	25	1

620



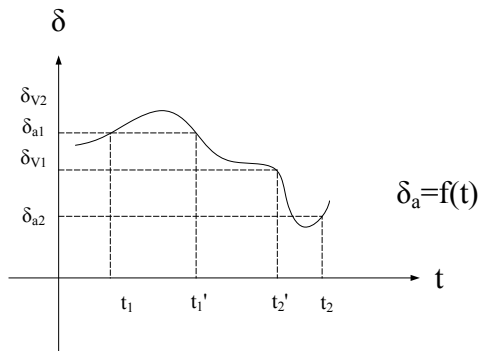
621



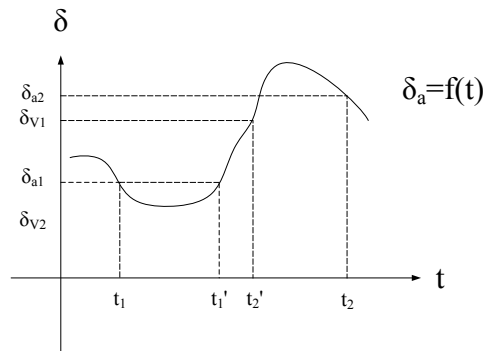
622

(a)

(b)



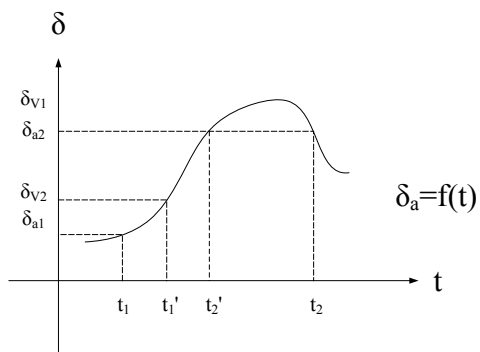
623



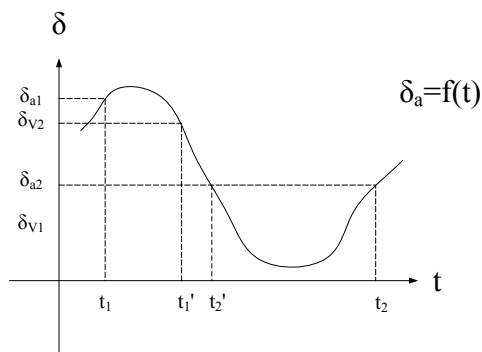
624

(c)

(d)



625



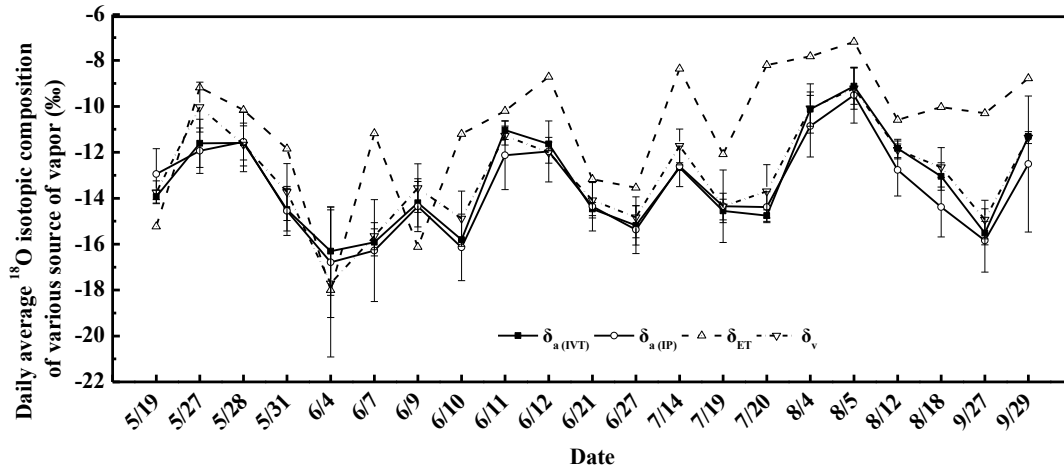
626

(e)

(f)

627 Fig. 1 Theoretical diagrams of all possible combinations of the relationships between isotope
 628 composition of ambient vapor (δ_a) and observed isotope composition of atmospheric vapor (δ_v)
 629 of two continuous moments t_1 and t_2 , ($t_1 < t_2$). δ_{a1} and δ_{a2} represent δ_a value in t_1 and t_2 ,
 630 respectively. δ_{v1} and δ_{v2} represent δ_v value in t_1 and t_2 , respectively. t_1' and t_2' represent the time
 631 of two specific moments between t_1 and t_2 with $t_1 < t_1' < t_2' < t_2$. For all of the six situations,
 632 there exists some sub-intervals $[t_1', t_2'] \subset [t_1, t_2]$ such that the whole range of $\{\delta_a(t) : t \in$
 633 $[t_1', t_2']\}$ is within $[\min(\delta_{v1}, \delta_{v2}), \max(\delta_{v1}, \delta_{v2})]$.

634



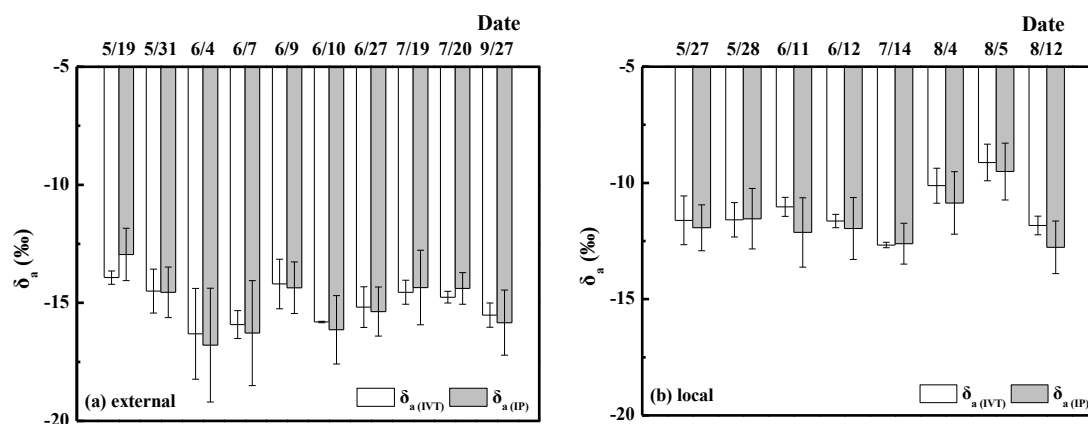
635

636

Fig. 2 The daily average values of the isotope composition of evapotranspiration vapor (δ_{ET}),
 637 the isotope composition of atmospheric vapor (δ_v), the estimated isotope composition of
 638 ambient vapor using the intersection point method ($\delta_{a(IP)}$) and the Intermediate Value Theorem
 639 method ($\delta_{a(IVT)}$) in the 21 days (see method section 2.3).

640

641



642

643 Fig. 3 The daily average values of the estimated isotope composition of ambient vapor using
644 the intersection point method ($\delta_{a(IP)}$) and the Intermediate Value Theorem method ($\delta_{a(IVT)}$) after
645 filter. Hybrid Single Particle Lagrangian Integrated Trajectory (HYSPLIT) backward trajectory
646 showed external origin (a) and local origin (b), respectively.

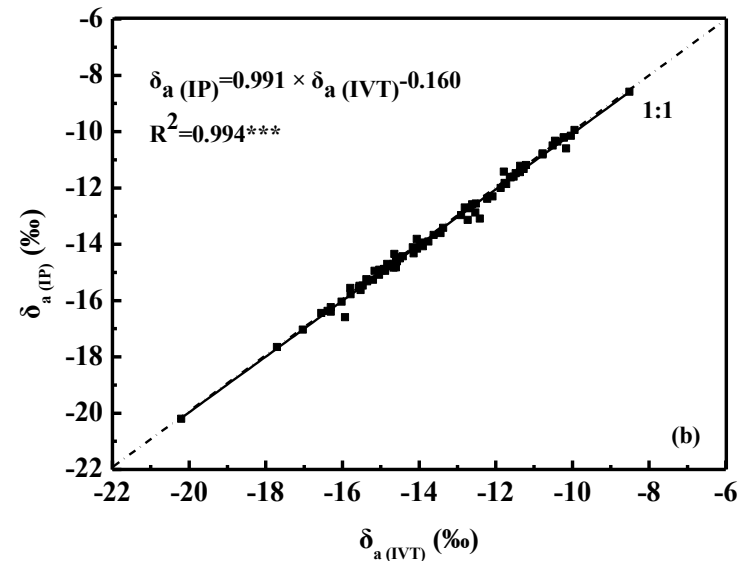
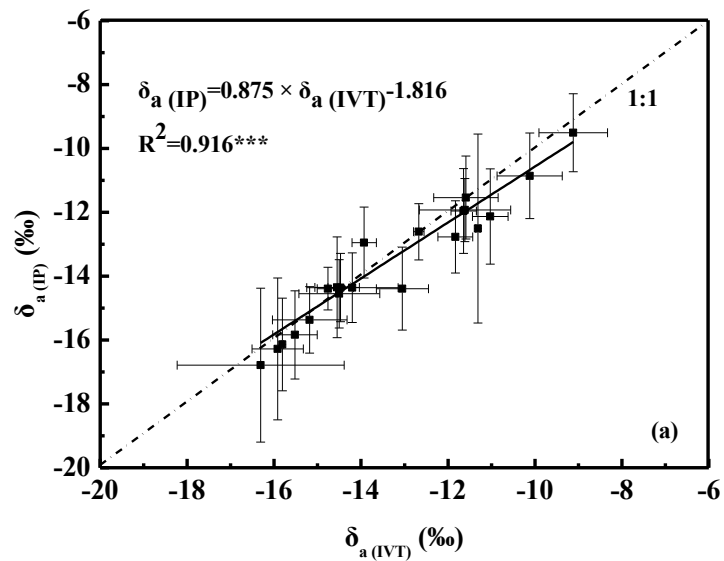


Fig. 4 Linear regression between the estimated isotope composition of ambient vapor using the intersection point method ($\delta_{a(\text{IP})}$) and the Intermediate Value Theorem method ($\delta_{a(\text{IVT})}$) on daily scale (a) and point to point scale (b), respectively.

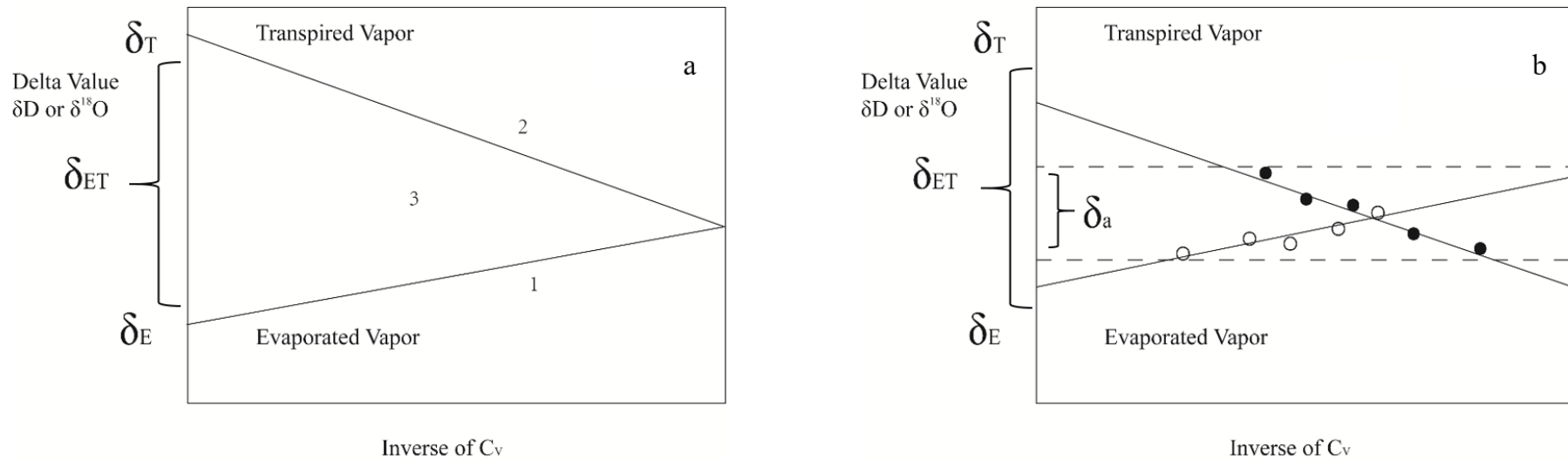


Fig. 5 Hypothetical graph of the idealized Keeling plots of the isotope composition of evaporation vapor (δ_E) (line 1), the isotope composition of transpiration vapor (δ_T) (line 2) and the isotope composition of evapotranspiration vapor (δ_{ET}) (area 3) (a), and hypothetical graph of idealized δ_E , δ_T lines and the interval of possible the isotope composition of ambient vapor (δ_a) in the Keeling plots (b).